Monthly Notices
of the
ROYAL ASTRONOMICAL SOCIETY

MNRAS **479,** 4279–4291 (2018)
Advance Access publication 2018 June 28

doi:10.1093/mnras/sty1645

Variable stars in local group galaxies – IV. RR Lyrae stars in the central regions of the low-density galaxy Crater II

M. Monelli,[1,2]★ A. R. Walker,[3]★ C. E. Martínez-Vázquez,[3] P. B. Stetson,[4] C. Gallart,[1,2] E. J. Bernard,[5] G. Bono,[6] A. K. Vivas,[3] G. Andreuzzi,[7] M. Dall'Ora,[8] G. Fiorentino[9] and A. Dorta[1,2]

[1]*Instituto de Astrofísica de Canarias, Calle Via Lactea, E-38205 La Laguna, Tenerife, Spain*
[2]*Universidad de La Laguna, Dpto. Astrofísica, E-38206 La Laguna, Tenerife, Spain*
[3]*Cerro Tololo Inter-American Observatory, National Optical Astronomy Observatory, Casilla 603, La Serena, Chile*
[4]*Dominion Astrophysical Observatory, Herzberg Institute of Astrophysics, National Research Council, Victoria, British Columbia V9E 2E7, Canada*
[5]*Université Côte d'Azur, OCA, CNRS, Lagrange, F-06304 Nice, France*
[6]*Departimento di Fisica, Universitá di Roma Tor Vergata, via della Ricerca Scientifica 1, I-00133 Rome, Italy*
[7]*Fundación Galileo Galilei – INAF, E-38712 Breña Baja, La Palma, Spain*
[8]*INAF – Osservatorio Astronomica di Capodimonte, salita Moiariello 16, I-80131 Napoli, Italy*
[9]*INAF – Osservatorio Astronomica di Bologna, via Ranzani 1, I-40127 Bologna, Italy*

Accepted 2018 June 18. Received 2018 June 18; in original form 2018 May 17

ABSTRACT

We present a search and analysis of variable stars in the recently discovered Crater II dwarf galaxy. Based on B, V, I data collected with the Isaac Newton Telescope (FoV$\sim$0.44 deg^2), we detected 37 variable stars, of which 34 are bone-fide RR Lyrae stars of Crater II (28 RRab, 4 RRc, 2 RRd). We applied the metal-independent (V, $B-V$) Period–Wesenheit relation and derived a true distance modulus ($\mu = 20.30 \pm 0.08$ mag ($\sigma = 0.16$ mag). Individual metallicities for RR Lyrae stars were derived by inversion of the predicted I-band Period–Luminosity relation. We find a mean metallicity of [Fe/H] $= -1.64$ and a standard deviation of $\sigma_{[Fe/H]} = 0.21$ dex, compatible with either negligible or vanishing intrinsic metallicity dispersion. The analysis of the colour–magnitude diagram reveals a stark paucity of blue horizontal branch stars, at odds with other Galactic dwarfs, and globular clusters with similar metal abundances.

Key words: stars: general – stars: horizontal branch – stars: variables: RR Lyrae – galaxies: evolution – Local Group.

1 INTRODUCTION

The last few years have revealed a completely new picture in our understanding of the Galactic neighborhood with the discovery of $\sim$20 dwarf galaxies surrounding the Milky Way, doubling the number of satellites known in 2014 (Bechtol et al. 2015; Drlica-Wagner et al. 2015; Kim et al. 2015; Kim & Jerjen 2015a,b; Koposov et al. 2015; Laevens et al. 2015a,b; Martin et al. 2015; Drlica-Wagner et al. 2016; Torrealba et al. 2016a,b, 2018; Koposov et al. 2018). Standing out among the new discoveries, the Crater II galaxy (Torrealba et al. 2016a) is not an ultra-faint compact satellite, but it is instead the fourth more extended galaxy around the Milky Way, following the two Magellanic Clouds and the Sagittarius dwarf spheroidal (dSph) galaxy. Crater II is, however, significantly fainter than those large galaxies, having an absolute magnitude of $M_V = -8.2$ mag (Torrealba et al. 2016a). With a surface brightness of only 31 mag arcsec^{-2}, Crater II is nearly invisible in a sea of field stars and lies close to the limits of detectability of current dwarf satellite searches (Koposov et al. 2008). No other Milky Way satellite has similar properties of brightness and size as Crater II although the plot of absolute magnitude versus radius given by Torrealba et al. (2016a, their fig. 6) shows that Andromeda XIX (McConnachie et al. 2008; Cusano et al. 2013) has similar surface brightness with slightly greater brightness and size.

The classical dSph galaxies surrounding the Milky Way have proven to be complex objects with varied, and different, star formation histories (SFHs, e.g. Mateo 1998; Tolstoy, Hill & Tosi 2009). No two dSph galaxies in our neighborhood are alike, and the reason(s) why they present such a variety of chemical enrichment and SFH is not well understood today. Study of the nature of these systems is fundamental for interpreting their role in the hierarchical process of formation of large galaxies such as our own Milky Way. Crater II presents then a unique opportunity to investigate the stellar

★ E-mail: monelli@iac.es (MM); awalker@ctio.noao.edu (ARW)

© 2018 The Author(s)
Published by Oxford University Press on behalf of the Royal Astronomical Society

Downloaded from https://academic.oup.com/mnras/article/479/4/4279/5046475 by CNRS - ISTO user on 07 June 2022

population and SFH in a galaxy unlike any other presently known among the Milky Way satellite galaxies.

The colour–magnitude diagram (CMD) of Crater II in its discovery paper (Torrealba et al. 2016a) shows a strong red giant branch (RGB) and horizontal branch (HB). Comparison with isochrones suggests that age of 10 Gyr and metallicity of [Fe/H] = –1.7 represent the data reasonably well. However, the depth of such CMD, limited to ∼0.5 mag below the HB, is inadequate to answer the critical question of the extent of the SFH of Crater II. The Carina dSph galaxy, for example, also presents a narrow RGB but deep CMDs clearly show a complex SFH with multiple main-sequence turnoffs and sub-giant branches (Monelli et al. 2003).

Spectroscopy by Caldwell et al. (2017) of 62 stars nominated as members selected from a sample close to the RGB in the CMD show that Crater II has extremely cold dynamics, even though it is still dark matter dominated with mass-light ratio 53^{+15}_{-11} $M_{\odot}/L_{V,\odot}$. For these stars, they also determine a mean metallicity [Fe/H] = –2.0 ± 0.1 dex, with a resolved dispersion of $\sigma_{[Fe/H]} = 0.22^{+0.04}_{-0.03}$ dex. The photometric metallicity found from isochrone fitting by Torrealba et al. (2016a) is some 0.3 dex more metal rich.

Variable stars can also be used for studying the content and structure of stellar systems. The presence of RR Lyrae (RRL) stars, for example, is an unequivocal sign of an old stellar population (>10 Gyr; Walker 1989) and, in addition, allows an independent determination of distance (Marconi et al. 2015; de Grijs et al. 2017). Their period and mean magnitude distributions can shed light on the metallicity distribution and even provide hints on the SFH of the oldest populations (Martínez-Vázquez et al. 2016a). anomalous Cepheids (AC), which are common (but not very numerous) in dSph galaxies but not in Galactic globular clusters (GCs), are usually interpreted as belonging to an intermediate-age population (Fiorentino & Monelli 2012), although this interpretation needs care because of primordial binaries being an alternate production channel (Bono et al. 1997).

In this paper, we present a search for variable stars in the field of Crater II, independent from the very recent work by Joo et al. (2018). Section 2 presents a summary of the data and the data reduction strategy. Section 3 presents the CMD and discusses the stellar populations in Crater II. Section 4 discusses the search for variable stars and the properties of RRL stars. In Section 5, we discuss the distance to Crater II, based on the Period–Wesenheit relation, while in Section 6, we derive the RRL stars metallicity distribution. Section 7 provides a discussion of the results and final remarks.

2 OBSERVATIONS AND DATA REDUCTION

Observations were collected with the Isaac Newton Telescope (INT) located in the Observatorio Roque de los Muchachos (ORM) in La Palma (Spain) using the Wide Field Camera (WFC; FoV = 33.8 × 33.8 arcmin^2), under two programmes approved by the Spanish Time Allocation Committee: the Large Programme C143 and the service program SST2017-380 (P.I.: Monelli). The observations have been realized in three different runs, of four, two, and three nights, respectively (see Table 1 for more details). The area covered by these data is 37 × 62 arcmin^2, approximately centred on the galaxy, but only the central 0.44 deg^2 have a robust calibration. Therefore, this data set covers much less than half the entire body of Crater II ($r_h = 31.2'$, Torrealba et al. 2016a).

The data have been collected over a 311-d baseline. Given its declination (Dec. ∼ –18°.5), Crater II is visible with airmass <1.7 for only about 4 h per night at the ORM, which implies that long time-series in a single night could not be obtained. Nevertheless, the median (maximum) number of phase points per star is of 49 (75), 25 (48), and 62 (68) for the *B*, *V*, and *I* bands, respectively. Therefore, despite the time sampling being not optimal, for most of the stars identified as possible variables we have been able to derive light-curve parameters adequate for our purpose here, though we do not discard that some periods estimated in this work may be affected by aliasing problems.

The photometric analysis was carried out by PBS using software, procedures, and standard stars that have been extensively described in the literature (e.g. Stetson 2000, 2005).

Table 1. Log of observations.

Run dates	Telescope	Detector	*B*	*V*	*I*
2016 May 29–31	INT	WFC	13	9	10
2017 January 27–28	INT	WFC	21	39	20
2017 April 03	INT	WFC	41	–	38

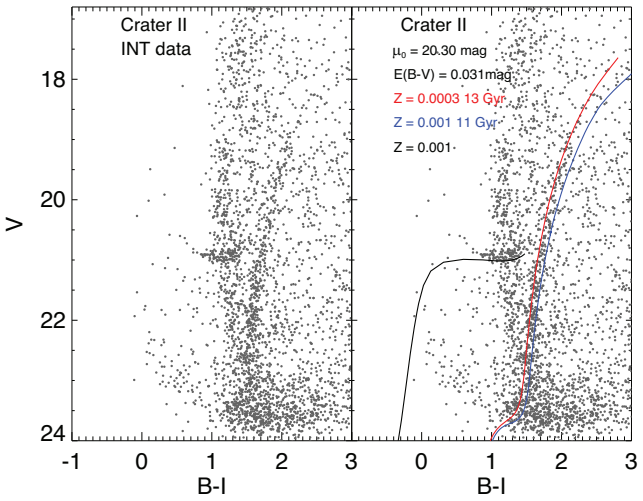


Figure 1. (*V*, *B* − *I*) colour–magnitude of the central region of Crater II. The bright portion of the RGB and the red HB are the most prominent features, together with a heavy contamination of field stars. The right-hand panels present the same CMD with superimposed old (13 Gyr and 10 Gyr) and metal-poor (Z = 0.0003, 0.001) isochrones from the BaSTI library. A ZAHB for Z = 0.001 is also plotted, shifted by 0.05 mag (Cassisi et al. 2007). These theoretical lines were shifted according with a distance modulus of 20.30 mag (see Section 5 for details) and a reddening of $E(B-V) = 0.027$ mag (Schlafly & Finkbeiner 2011).

3 COLOUR–MAGNITUDE DIAGRAM

Fig. 1 (left-hand panel) presents the (*V*, *B* − *I*) CMD of the region around the center of Crater II. The photometry reaches *V* ∼23.8 mag, and the plot shows a prominent contamination by the Galactic field, at color redder than *B* − *I* ∼1.0 mag. Nevertheless, the RGB and predominantly red HB are clearly visible in the CMD. To guide the eye (right-hand panel), we superimposed two α-enhanced isochrones from the BaSTI (Pietrinferni et al. 2004, 2006) database. We assumed the distance estimated in Section 5, and the red and blue lines show the expected location of a population of (Z, age in Gyr) = (0.0003, 13) and (0.001, 11), respectively. The black line shows the zero-age HB for Z = 0.001, which provides a nice lower envelope for the distribution of stars in the red part of the HB and for the RRL stars.

Downloaded from https://academic.oup.com/mnras/article/479/4/4279/5046475 by CNRS - ISTO user on 07 June 2022

The comparison with isochrones clearly shows that these data are too shallow to detect stars at the turn-off (TO). Nevertheless, a sequence of blue objects ($B - I < 1$, $V > 22$ mag) is well defined between the HB and the TO. Most likely, it is populated by Blue Stragglers, as commonly found in all dSph galaxies (Mapelli et al. 2007, 2009; Monelli et al. 2012b; Santana et al. 2013). However, based on the present data, we cannot robustly constrain the youngest age at the TO, so we cannot exclude the presence of a small intermediate age component. Interestingly, the HB of Crater II is mostly red, with very few, if any, stars bluer than the instability strip.

4 VARIABLE STARS IN CRATER II

4.1 Search and classification

The search for candidate variable stars has been realized using the method introduced by Welch & Stetson (1993) and as further developed by Stetson (1996). The pulsational properties were estimated following Bernard et al. (2009). In particular, a first guess of the period is derived through Fourier analysis of the time series (Horne & Baliunas 1986), and then refined by simultaneous visual inspection of the light curves in all the available filters. Amplitudes are then estimated by fitting to a set of light-curve templates (Layden et al. 1999).

4.2 RRL stars

We identified 58 candidate variable stars, of which 37 are confirmed pulsators. Out of those 37 stars, 34 of them are RRL stars. Table 2 presents the full catalogue, including name,[1] coordinates (right ascension and declination), period, classification, followed by intensity-weighted mean magnitude and amplitude in the *B*, *V*, and *I* pass-bands, respectively. The last two columns show the period estimate by Joo et al. (2018) and notes on individual stars. One variable, V098, was not reported in Joo et al. (2018). We note that two of the stars (V023 and V056) had already been reported in the first release of PANSTARR (#204928 and #204866), though they were not associated to Crater II (Sesar et al. 2017). Time series photometry for the variable stars detected in this work is listed in the Appendix. Fig. 2 presents the *B* (blue), *V* (green), and *I* (red) light curves of all the discovered RRL variable stars.

After the submission of this work, Joo et al. (2018) published an independent investigation on the variable stars content of Crater II, based on KMTNet data covering $3^\circ \times 3^\circ$ in *B* and *V*. All variable stars in the overlapping area are in common between the two photometries except two: Based on our data, we cannot confirm the variability of V093, while we identify a new variable not listed in the Joo et al. (2018) catalogue (V098). The comparison of period estimates discloses a good agreement for most of the stars: the period difference is smaller than 0.05 d for 32 out of 36 stars (88 per cent). Four stars presents larger period differences, between 0.05 and 0.29 d, which is likely due to aliasing. We detected a small shift in the mean magnitude. The derived mean magnitudes for our full sample are $\langle B \rangle = 21.30 \pm 0.09$ ($\sigma = 0.09$) mag, $\langle V \rangle = 20.92 \pm 0.07$ ($\sigma = 0.05$) mag, and $\langle I \rangle = 20.34 \pm 0.06$ ($\sigma = 0.05$) mag, while both the $\langle B \rangle$ and $\langle V \rangle$ of the stars from Joo et al. (2018) in common with ours are ∼0.03 mag fainter.

[1] We assumed the naming convention by Joo et al. (2018).

Fig. 3 shows a zoom-in view of the CMD in the region of the HB. The RRL stars are shown as large symbols, with different colours indicating different pulsation modes: blue, green, and orange correspond, respectively, to the 4 first-overtone (RRc), 2 double-mode (RRd), and the 28 fundamental-mode (RRab) RRL stars discovered in this work. Three stars are well separated in magnitude from the bulk of the RRL stars. V097 and V098 are, respectively, 0.4 and 0.3 mag fainter than the HB. V098 has a period near 0.5 d and an RRc-like light curve, with a large phase gap. Additionally, inspecting its image shows it may be superimposed on a faint background spiral galaxy. V097 has a typical RRc period. V001 is 0.5 mag brighter than the HB, with periods and colours typical for an RRL star. It looks too faint to be an AC, which are typically at least 1 mag brighter than the HB, and its period is too short ($P = 0.763306$ d) to be a BL Her star (Di Criscienzo et al. 2007). Stars in this position of the HB are known in other systems (Carina: Coppola et al. 2015; Sculptor: Martínez-Vázquez et al. 2016b) and may be stars in the final stage of core helium-burning evolution evolving rapidly towards the AGB. Following the nomenclature introduced in Martínez-Vázquez et al. (2016b) for stars with similar behaviour as this one, we classified V001 as 'peculiar' variable star. We will not include these three stars in the subsequent analysis.

Fig. 4 presents the spatial distribution of RRL stars. The colour code is the same as in Fig. 1. The red cross marks the position of the center of Crater II according to Torrealba et al. (2016a). Interestingly, RRL stars seem to be spread over the full surveyed field, with no obvious concentration towards the central regions.

Fig. 5 shows the period–amplitude (Bailey) diagram (top panel) and the period distribution (bottom) for the full sample of RRL stars. Lines in the top panel present a comparison with the Oosterhoff I (Oo-I, solid) and II (Oo-II, dashed) loci, as defined for RRab type stars in GCs (Cacciari et al. 2005), and for RRc type (dotted, Kunder et al. 2013). The mean period $\langle P_{RRab} \rangle = 0.617$ d, which would suggest that Crater II is somewhat more similar to an Oo-II system, though it is at the edge of the so-called Oosterhoff gap typically populated by dSph galaxies. Nevertheless, the top panel of Fig. 5 clearly shows that RRab are distributed closer to the Oo-I line, though they seem to follow a steeper relation. This translates into a period distribution (bottom panel) that is quite narrow around the peak. Therefore, the lack of RRab with shortest period and largest amplitude mimics an Oo-II type if only the mean period is considered, but clearly the location of stars in the period–amplitude plane is closer to that of a Oo-I system. Many other low-mass, metal-poor systems are characterized by similar period distributions, lacking the short-period tail (e.g. Bootes: Siegel 2006; And XI and And XIII: Yang & Sarajedini 2012; And XIX: Cusano et al. 2013; And III: Martínez-Vázquez et al. 2017).

Fig. 5 suggests that the distribution of Crater II stars in the period–amplitude plane follows a distribution steeper than the Oo-I line. This is similar to what is observed in other systems such as Carina (Coppola et al. 2015), And III (Martínez-Vázquez et al. 2017), and Cetus (Monelli et al. 2012a). This is illustrated in Fig. 6, which compares the Baily diagram (top) of these three galaxies (orange points) with that of Crater II (black dots). Blue dots show RRL stars in Tucana (Bernard et al. 2009) and Sculptor (Martínez-Vázquez et al. 2016b, their *clean* sample). The plot shows that for amplitude close to 1 mag the orange points tend to split from the clusters'Oo-I line. The normalized period distribution (bottom panel) of Crater II RRab stars is remarkably similar to that of Carina+Cetus+And III, while Sculptor and Tucana present a more extended tail, especially at short-period end.

Downloaded from https://academic.oup.com/mnras/article/479/4/4279/5046475 by CNRS - ISTO user on 07 June 2022

Table 2. Variable stars properties.

Name	RA h m s	Dec. ° ′ ″	Period (d)	m_B	A_B (mag)	m_V	A_V (mag)	m_I	A_I (mag)	Type (mag)	P_{Joo} (d)	Notes
V001	11:48:46.94	−18:37:28.8	0.7633058	20.925	0.984	20.553	0.820	19.950	0.503	Peculiar	0.7633	
V002	11:48:59.49	−18:10: 9.8	0.6043024	21.432	0.913	20.966	0.759	20.406	0.546	RRab	0.6053	
V003	11:48:38.77	−18:31:40.2	0.6009024	21.217	1.019	20.920	0.834	20.349	0.515	RRab	0.6009	
V004	11:48:51.17	−18:16:34.1	0.4091809	21.260	0.477	20.906	0.470	20.403	0.218	RRc	0.4189	
V005	11:48:51.89	−18:31:56.7	0.5989511	21.227	1.229	20.904	0.966	20.335	0.575	RRab	0.5989	
V008	11:48:47.01	−18:31:30.5	0.6497012	21.217	0.679	20.907	0.504	20.305	0.372	RRab	0.6496	a
V010	11:47:51.72	−18:11:12.1	0.6113311	21.228	1.068	20.850	0.851	20.213	0.745	RRab	0.6212	b
V012	11:48:41.01	−18:31:45.4	0.6404212	21.375	0.766	20.968	0.687	20.340	0.492	RRab	0.6415	c
V013	11:48:51.59	−18:41:34.0	0.6486312	21.314	0.851	20.884	0.665	20.301	0.430	RRab	0.6474	
V014	11:48:39.64	−18:09:24.1	0.6090211	21.310	0.735	20.906	0.816	20.329	0.390	RRab	0.6081	c
V015	11:47:57.04	−18:08:39.6	0.5912911	21.289	0.917	20.904	0.624	20.280	0.424	RRab	0.6378	b; d ; e
V020	11:48:35.41	−18:30:54.6	0.6170524	21.370	0.673	20.956	0.491	20.301	0.315	RRab	0.6201	f; a
V021	11:49:05.76	−18:32:02.9	0.5960023	21.432	0.581	21.053	0.645	20.416	0.562	RRab	0.641	
V022	11:48:14.91	−18:15:09.1	0.6362525	21.096	1.603	20.816	1.133	20.361	0.435	RRab	0.6001	b; e
V023	11:48:10.63	−18:17:42.7	0.6122524	21.323	1.055	20.944	0.808	20.448	0.071	RRab	0.6147	b; e
V025	11:49:05.83	−18:40:46.9	0.6093524	21.310	1.080	20.909	0.826	20.366	0.516	RRab	0.6083	a
V029	11:49:23.49	−18:20:08.5	0.3997510	21.204	0.320	20.827	0.382	20.279	0.172	RRd	0.4212	
V033	11:49:45.65	−18:32:56.2	0.4284515	21.219	0.603	20.949	0.335	20.345	0.264	RRd	0.4174	
V035	11:49:56.30	−18:37:43.0	0.6309025	21.260	0.714	20.879	0.600	20.255	0.444	RRab	0.6309	
V046	11:49:36.81	−18:35:26.6	0.5931521	21.258	1.153	20.906	0.815	20.413	0.537	RRab	0.6155	g; a
V050	11:49:46.72	−18:32:12.9	0.5839523	21.070	1.466	20.875	0.745	20.336	0.625	RRab	0.5877	g
V052	11:49:40.58	−18:19:04.4	0.6290411	21.319	0.996	20.937	0.864	20.357	0.543	RRab	0.6280	
V056	11:49:44.85	−18:35:02.3	0.5666522	21.184	1.264	20.876	1.008	20.394	0.746	RRab	0.5658	
V057	11:49:53.68	−18:16:39.4	0.6324525	21.460	0.726	21.021	0.602	20.383	0.411	RRab	0.6314	g
V065	11:47:45.07	−18:23:27.0	0.6500526	21.296	0.748	20.891	0.590	20.293	0.454	RRab	0.6513	g
V066	11:49:47.00	−18:27:20.8	0.6203024	21.304	0.875	20.925	0.689	20.333	0.374	RRab	0.6268	
V068	11:49:12.51	−18:19:36.5	0.6525526	21.379	0.486	20.967	0.382	20.330	0.317	RRab	0.6478	
V070	11:49:12.03	−18:15:50.3	0.6222525	21.342	0.904	20.912	0.751	20.311	0.514	RRab	0.6245	h
V072	11:48:49.98	−18:28:27.5	0.3913809	21.347	0.379	20.980	0.240	20.372	0.143	RRc	0.6553	d
V073	11:49:30.21	−18:41:32.3	0.6457655	21.357	0.720	20.910	0.472	20.335	0.343	RRab	0.6493	
V076	11:49:04.08	−18:09:07.6	0.4063514	21.406	0.413	21.028	0.266	20.401	0.231	RRc	0.6516	d; e
V077	11:49:17.36	−18:38:55.8	0.6132524	21.266	0.941	20.911	0.781	20.336	0.470	RRab	0.6132	
V078	11:49:16.90	−18:33:54.2	0.6190025	21.403	0.865	21.007	0.507	20.437	0.447	RRab	0.6029	c
V083	11:48:45.47	−18:09:58.5	0.6208012	21.382	1.197	20.916	0.818	20.350	0.518	RRab	0.6229	
V092	11:48:58.03	−18:22:07.7	0.4149109	21.247	0.372	20.850	0.223	20.263	0.173	RRc	0.7084	f
V097	11:49:16.15	−18:18:35.4	0.3067604	21.625	0.649	21.322	0.406	20.867	0.364	uncertain	0.2347	d
V098	11:48:38.19	−18:35:39.7	0.5095519	21.664	0.454	21.212	0.300	20.725	0.261	uncertain	–	d

Notes. *a* – lack of maximum in *I* band.
b – only few points/phase in *I* band.
c – candidate Blazhko.
d – noisy light curves.
e – many possible periods.
f – noisy light curve in *I* band.
g – lack of maximum in *V* band.
h – lack of maximum.

5 DISTANCE TO CRATER II

RRL stars are primary, fundamental distance indicators (Carretta et al. 2000; Cacciari & Clementini 2003). The well-known metallicity–luminosity relation (Sandage, Katem & Sandage 1981) has been extensively used in the literature, applied to GCs (Arellano Ferro et al. 2008; Di Criscienzo et al. 2011; di Criscienzo et al. 2011; McNamara 2011) and nearby dwarf galaxies (e.g. Stetson et al. 2014; Yang et al. 2014; Cusano et al. 2016, 2017; Martínez-Vázquez et al. 2016a). Nevertheless, this relation is subject to many sources of uncertainties (linearity, evolutionary effects, and reddening; Bono 2003), though the most important one comes from the fact that neither the zero point nor the slope has been definitively calibrated (de Grijs et al. 2017). This translates into a difference of up to ∼0.2 mag according to the adopted calibration (Chaboyer 1999; Bono et al. 2003; Clementini et al. 2003).

Alternatively, period–luminosity relations (Longmore, Fernley & Jameson 1986; Bono et al. 2001) in the near infrared present important advantages, such as the significantly milder dependency on the reddening and evolutionary effects. The exhaustive theoretical work by Marconi et al. (2015) discusses in detail the use of period–luminosity–metallicity (PLZ) relations of RRL stars to derive the distance of the host stellar system. In particular, the Wesenheit functions (Madore 1982) are particularly useful because, by construction, they are reddening independent, given the assumption of a reddening law. Moreover, Marconi et al. (2015) showed that the (V, $B - V$) Wesenheit relation presents the remarkable property of also being independent of metallicity, over a wide range.

Downloaded from https://academic.oup.com/mnras/article/479/4/4279/5046475 by CNRS - ISTO user on 07 June 2022

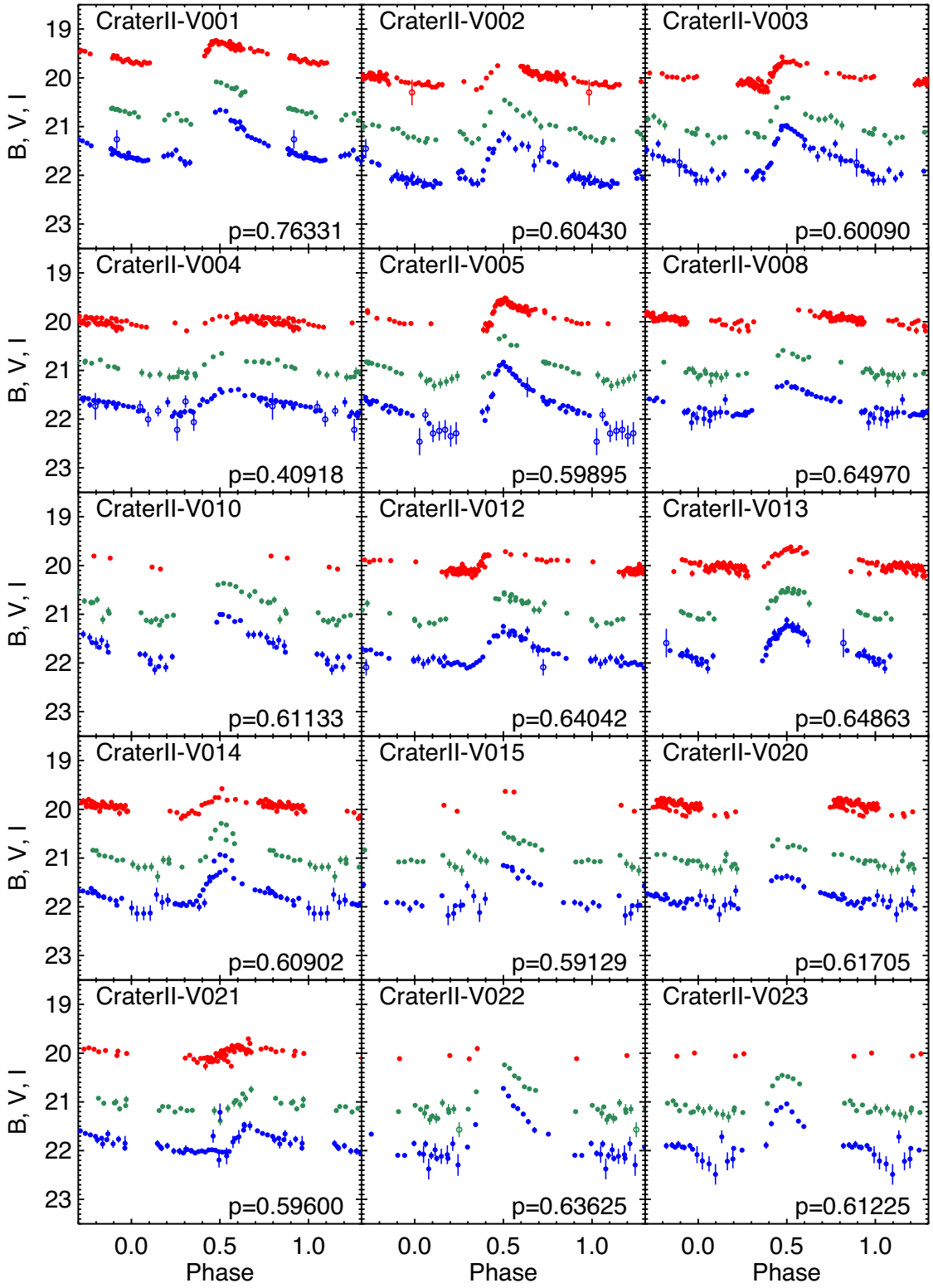


Figure 2. *B* (blue), *V* (green), and *I* (red) light curves for variable stars in Crater II. Star names (upper left-hand corner) are sorted for increasing right ascension. Periods (lower right-hand corner) are given in days. Open symbols (not used in the estimation of the pulsation properties) show the data for which the uncertainties are larger than 3σ above the mean error of a given star. Note that *B* and *I* light curves were shifted by +0.4 and –0.4 mag, respectively, to facilitate the visual inspection of all three together.

Downloaded from https://academic.oup.com/mnras/article/479/4/4279/5046475 by CNRS - ISTO user on 07 June 2022

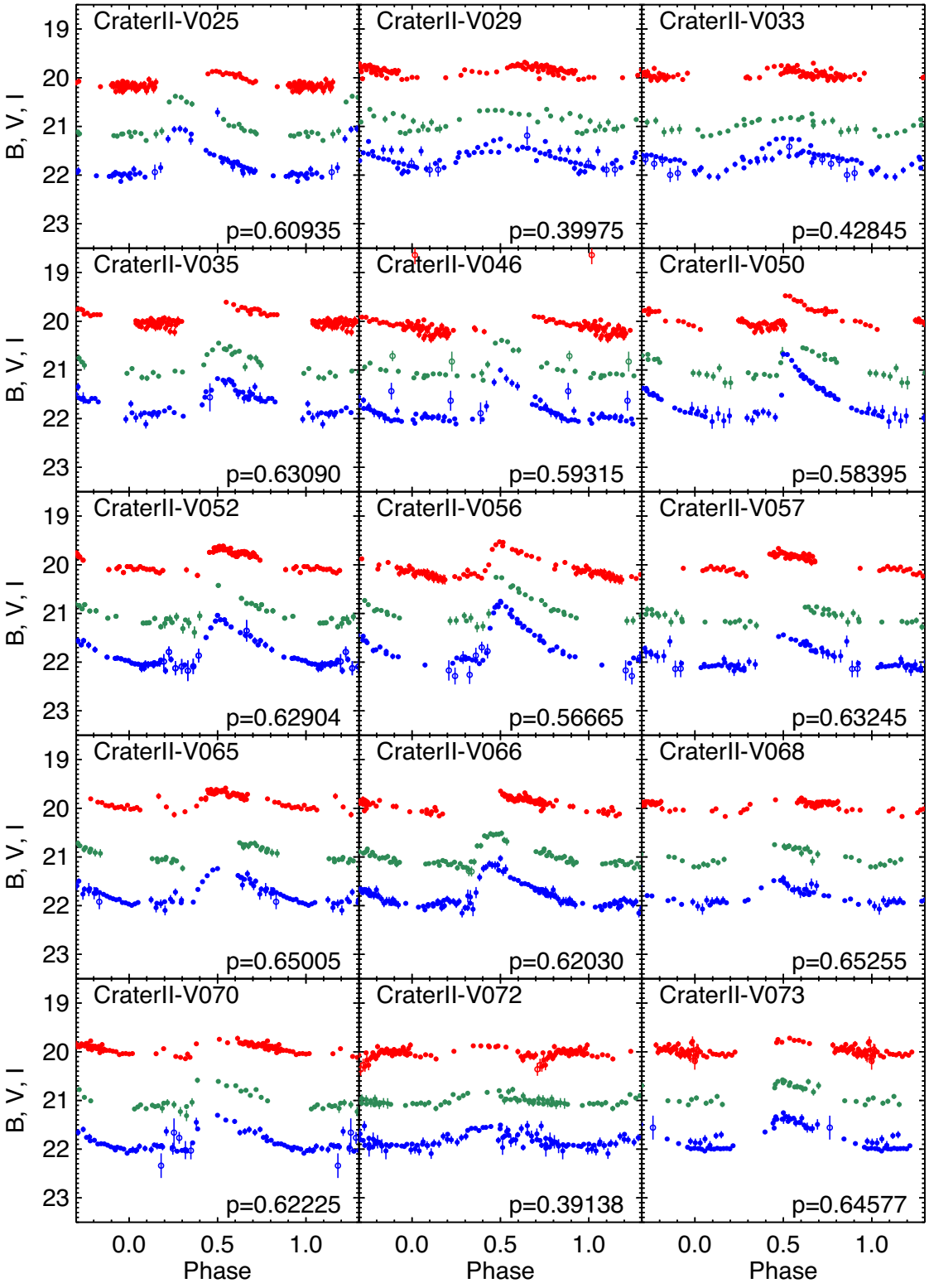


Figure 2. continue.

Downloaded from https://academic.oup.com/mnras/article/479/4/4279/5046475 by CNRS - ISTO user on 07 June 2022

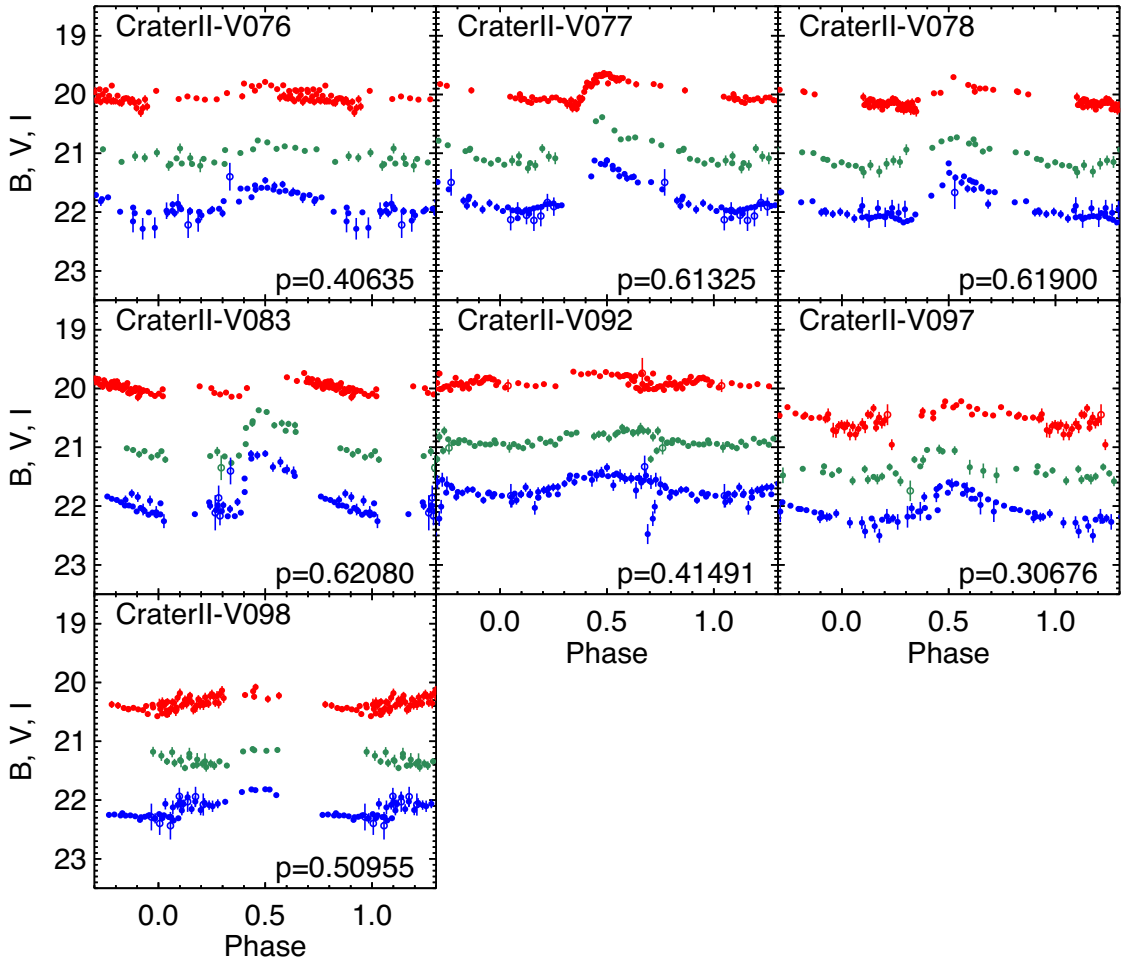


Figure 2. continue.

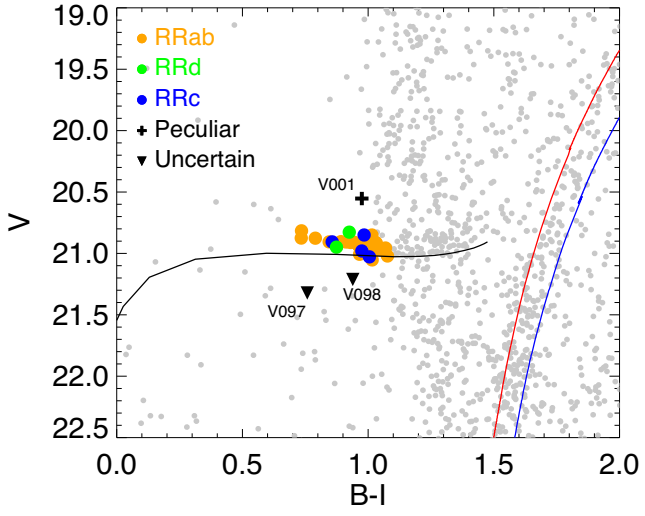


Figure 3. Zoom-in view of the (V, $B - I$) colour–magnitude of Crater II centered on the HB location. The discovered RRL stars are shown with filled symbols, splitting RRab (orange), RRc (blue), and RRd (green) type stars. The same isochrones and ZAHB as in Fig. 1 are shown.

This implies that a possible intrinsic metallicity dispersion, such as that found in the local group dwarf galaxies Tucana (Bernard et al. 2008) and Sculptor (Martínez-Vázquez et al. 2015), does not affect the distance determination.

We adopted the ($V, B - V$) Wesenheit relation from Marconi et al. (2015) and derived the distance modulus to Crater II, obtaining $(m - M)_0 = 20.30 \pm 0.08$ mag ($\sigma = 0.16$ mag). This is illustrated in Fig. 7, which shows the W($V, B - V$) magnitude as a function of the logarithm of the period for 28 RRL stars. The peculiar, two uncertain, and the three Blazkho stars have been excluded, and the period of the remaining four RR*c* type has been fundamentalized. The result is in good agreement with the value provided by Torrealba et al. (2016a), $(m - M) = 20.35$, based on the comparison with theoretical isochrones and with the distance estimated by Joo et al. (2018) based on a larger sample of RRL stars, $(m - M)_0 = 20.25 \pm 0.1$.

6 METALLICITY DISTRIBUTION

Martínez-Vázquez et al. (2016a) and Braga et al. (2016) introduced the use of the *I*–PLZ relation as a metallicity rather than a distance indicator. If the distance is provided by an independent indicator, the individual metallicity can be calculated for each RRL star, given its absolute M_I magnitude and period. In the case of the current data

Downloaded from https://academic.oup.com/mnras/article/479/4/4279/5046475 by CNRS - ISTO user on 07 June 2022

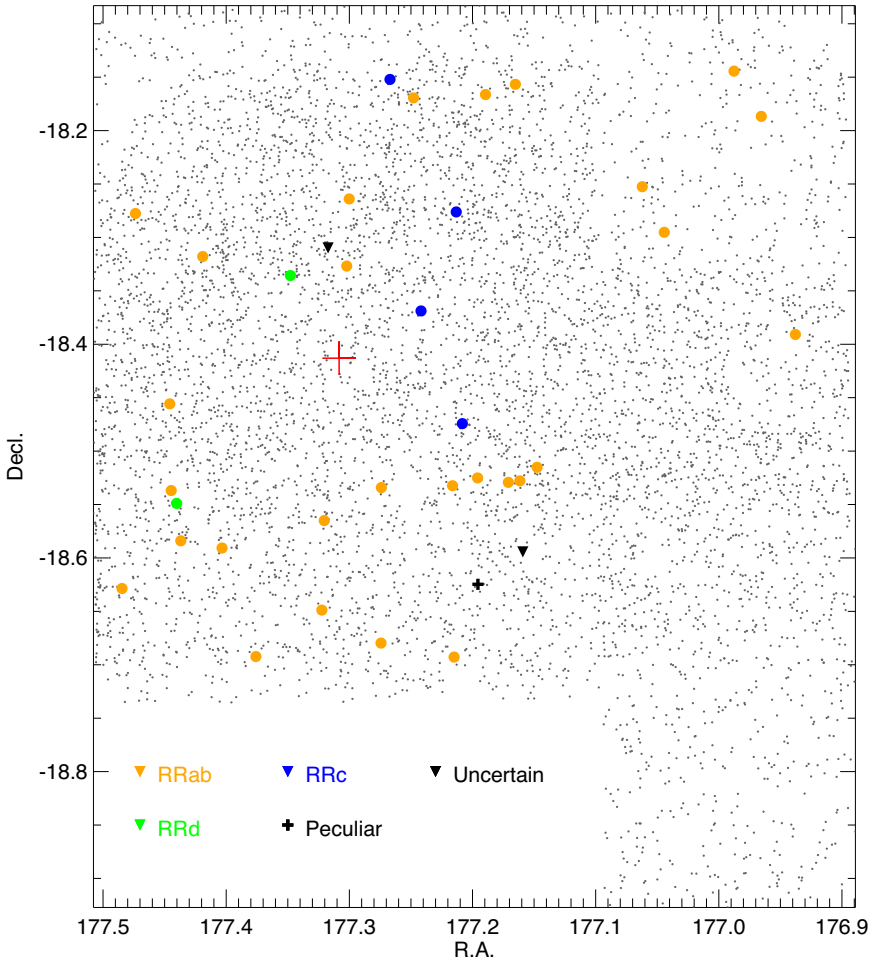


Figure 4. RRL variable stars in the field of Crater II. The colour code is the same as in Fig. 3. Black symbols indicate the position of the peculiar and uncertain stars. The nominal center of the galaxy (red cross) is taken from Torrealba et al. (2016a).

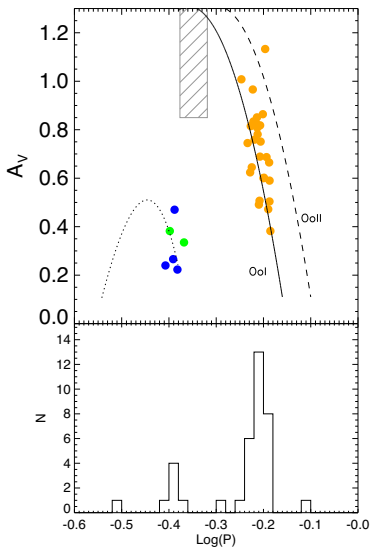


Figure 5. Top panel: period–amplitude Bailey diagram for the 32 RRL stars in the central region of Crater II. We overplotted the Oosterhoff sequences for fundamental pulsators from Cacciari, Corwin & Carney (solid and dashed line for OoI and OoII, respectively, 2005) and for first overtone from Kunder et al. (2013). Bottom panel: Period distribution for the RRL stars plotted in the top panel.

set, we can take advantage of the three filters available: *B*, *V*, and *I*. First, we adopted the metal-independent distance estimate based on the W(V, $B - V$) Wesenheit function derived in Section 5. This was used to derive an absolute *I* magnitude for each RRL star. Secondly, we applied the inverse of the *I*–PLZ relation to derive individual metallicity (rather than individual distances as typically done). The derived metallicty distribution for RRL stars is shown as a normalized dashed histogram in Fig. 8.

We derived individual metallicities for a sample of 21 RR*ab* stars with good light curves. We did not include first overtone pulsators, the peculiar star, the Blazhko ones, the two candidates, and four stars with poorly constrained light curve in the *I* band (V010, V015, V022, and V023). The distribution covers a range between [Fe/H] $\sim$ –2.2 and [Fe/H] $\sim$ –1.2 dex, and appears symmetric around a well defined peak. A Gaussian fit to the distribution provides a mean metallicity [Fe/H] = –1.64 dex, with a dispersion σ = 0.21 dex. Martínez-Vázquez et al. (2016a) discussed the resolution of the method by analysing the population of RRL stars of GCs with no spectroscopically measured intrinsic metallicity spread. The metallicity distribution derived for 22 RRL stars in the LMC cluster Reticulum provided a dispersion $\sigma = 0.25$ dex. This suggests that the intrinsic metallicity dispersion of RRL stars in Crater II is compatible with being basically null. It is also worth stressing that the adopted distance affects the metallicity estimate as a zero point:

Downloaded from https://academic.oup.com/mnras/article/479/4/4279/5046475 by CNRS - ISTO user on 07 June 2022

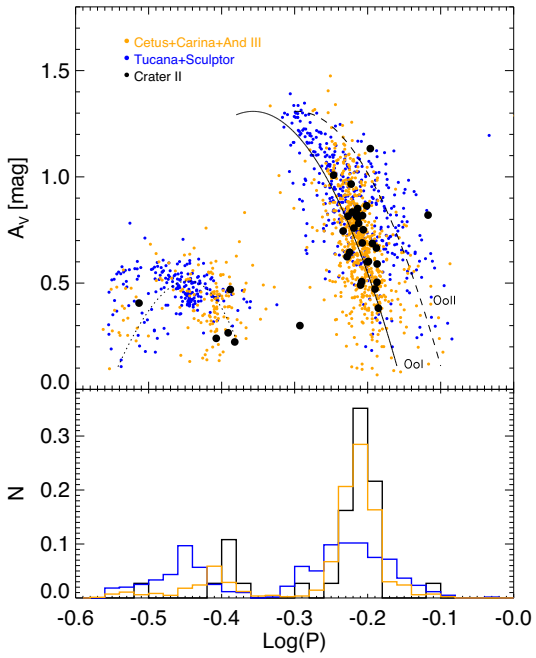


Figure 6. Comparison of the Bailey diagram of different galaxies. Orange symbols show the position of star in Carina, And III, and Cetus, which present a steeper relation, similar to that of Crater II (black), with respect of Sculptor and Tucana (blue points).

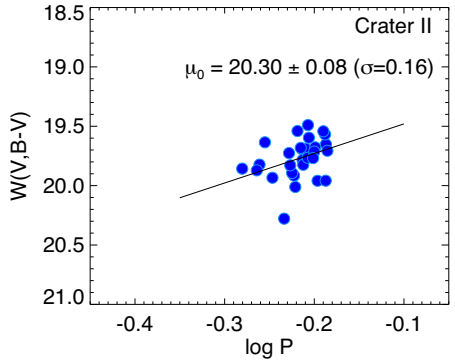


Figure 7. W(V, $B - V$)–log P relation for the 24 RRab and the 4 fundamentalized RRc, in Crater II. The black line is the fit of the data to the theoretical slope predicted by Marconi et al. (2015). The zero-point of this relation gives us the first estimation of the distance modulus (μ_0) for Crater II based on a standard candle.

Longer distances produce a more metal-poor distribution (by 0.6 dex for a 0.1 mag shift). However, the distribution shape, hence its dispersion, is unaffected.

The derived mean metallicity is in good agreement with that found by Joo et al. (2018), $\langle$[Fe/H]$\rangle = -1.65 \pm 0.15$ on the basis of the period–amplitude–metallicity relation by Alcock et al. (2000), though our dispersion ($\sigma = 0.21$ dex) is smaller than their value ($\sigma = 0.31$ dex). The red histogram in the Fig. 8 shows the metallicity distribution of the 62 stars identified by Caldwell et al. (2017) as bona-fide members of Crater II on the basis of their radial velocity and proximity to the nominal Crater II RGB. Metallicity estimates have been homogeneized to the same scale, correcting for the different solar abundances adopted (log([Fe/H])/log([Fe/H])$_\odot$ = 7.50). The comparison discloses substantial agreement between the two,

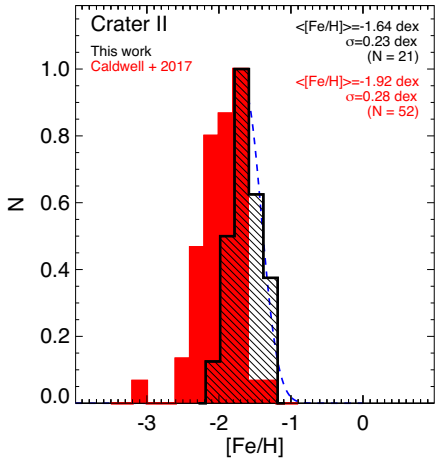


Figure 8. Metallicity distribution of 19 RRL stars in Crater II as derived from the theoretical *I*–PLZ relation presented in (Marconi et al. 2015). The red histogram shows the metallicity of 52 derived spectroscopically by Caldwell et al. (2017).

completely independent, estimates. A gaussian fit provides similar dispersion ($\sigma = 0.28$ versus 0.21), with the value from RGB stars slightly smaller than for the RRL stars. The small offset between the two distributions can be explained by the 0.05 mag difference in the distance adopted (20.35 versus 20.30 mag), and it is well within the uncertainties. Apparently, the spectroscopic sample presents a more extended tail to the metal-poor side. We verified that this is not due a variation in the characteristics of the stellar populations with radius, since the Caldwell et al. (2017) sample covers a wider area of Crater II. The difference is possibly due to a random fluctuation due to the relatively small sample of RRL stars used.

Overall, the metallicity distribution of a purely old sample of RRL stars is similar to that of RGB stars, which, in principle, can include populations younger and/or too metal-rich to have counterparts in the RRL stars population. This suggests that Crater II experienced a quick (within the formation time scale of RRL stars progenitors) and limited chemical evolution. This is supported by the lack of high-amplitude short-period RRL stars (Fiorentino et al. 2015). These stars are a strong indication that their progenitors belong to a population at least as metal-rich as [Fe/H] $= -1.5$ dex. The Bailey diagram of Crater II is devoid of such stars ($P_{ab,\,min} = 0.566\,652$d), suggesting that the upper limit to the metallicity distribution of RRL stars is significantly lower than [Fe/H] $= -1.5$ dex (Fiorentino et al. 2017).

7 DISCUSSION AND FINAL REMARKS

Crater II is a dwarf galaxy with many fascinating properties. The galaxy size–magnitude plot (e.g. Torrealba et al. 2016a) shows no other MW satellite with similar properties. It is the fourth most physically extended MW satellite ($r_h \approx 1$ kpc) (after the Magellanic Clouds and Sagittarius) *and* one of the galaxies with the lowest known surface brightness ($\mu_V \sim 31.2$ mag). Only Andromeda XIX lies in a similar position in this plot. Therefore, Crater II appears as either overlarge or underluminous, compared to most other LG galaxies.

Analyzing INT/WFC data, we have found a substantial population of RRL stars in the central regions of Crater II. The RRL stars that we have discovered lack any central concentration and are widely distributed over our whole field. Thus, our sample of

Downloaded from https://academic.oup.com/mnras/article/479/4/4279/5046475 by CNRS - ISTO user on 07 June 2022

variable stars is likely incomplete and indicates that the galaxy extends outside the surveyed field of view. This was already expected, given the stellar distribution in the discovery paper (Torrealba et al. 2016a).

Interestingly, our search for variable stars did not reveal any ACs in the central regions of Crater II. Assuming the empirical relation found by Mateo, Fischer & Krzeminski (1995) between the fraction of ACs and the luminosity of the host galaxy, one would expect very few of them, at most 1–2 for $M_V = -8$ mag (Torrealba et al. 2016a). Fiorentino & Monelli (2012) argued that this relation may be used to identify dwarf galaxies with an important fraction of intermediate-age population, as in this case the number of ACs increases with respect to a purely old sample descending from primordial binary stars. In this sense, the absence of ACs in Crater II can be compared to the sizable samples detected in galaxies of similar luminosity, such as And XIX, which hosts eight AC (Cusano et al. 2013), possibly indicating a significant intermediate age population, and Leo T (Clementini et al. 2012), where indeed a strong intermediate-age population is present. This may be considered indirect evidence that Crater II has a negligible, if any, younger population.

Comparison with theoretical isochrones supports this conclusion and suggests that the bulk of star formation in Crater II occurred at an early epoch. The presence of a sequence of objects bluer and brighter than the TO of the old population is compatible with a population of BSS. Nevertheless, deeper data are necessary in order to set stronger constraints on the quenching epoch and on the existence of a minority intermediate-age population.

The metallicity derived from a sample of 21 RRL stars reveals a narrow distribution peaked at [Fe/H] $= -1.64$, with an observed dispersion compatible with a negligible intrinsic dispersion. The chemical properties of RRL stars are in agreement with those of the sample of 62 RGB stars investigated by Caldwell et al. (2017), both in terms of mean metallicity and dispersion. Since the RGB can be populated by a mix of populations with a significantly broader range of age and metallicity than a purely old sample of RRL stars, this suggests that Crater II does not host any strong population significantly more metal-rich than the RRL stars. Similarly, the narrow metallicity distribution may suggest the absence of a significant tail of very low metallicity stars such as are found in other dwarf galaxies of similar brightness, like Eridanus II (Li et al. 2017) or CVnI (Kirby et al. 2008).

Finally, a striking feature in the CMD of Crater II is the morphology of the HB. In fact, while the red HB is well-populated, only a handful of objects are located in the region of the blue HB, for stars cooler than $0.0 < B - I < 0.5$ mag. This is a strong peculiarity compared to bright MW satellites, which *always* present a sizable sample of RRL stars together with a well-populated HB for colours bluer than the instability strip. This is true independently of the details of the early SFH. This occurrence is present in the most metal-poor systems such as Ursa Minor (which has the bluest HB), but also in those with strong intermediate-age component such as Carina, Fornax, or Leo I. Despite the redder, on average, HB morphology (Da Costa et al. 1996, 2000; Da Costa, Armandroff & Caldwell 2002), such an extreme case is not common among the M31 satellites either. The analysis of 20 galaxies by Martin, Ibata & Irwin (2007) suggests that only And XXIV may lack blue HB stars. Interestingly, the luminosity of And XXIV and the metallicity ([Fe/H] $= -1.8 \pm 0.2$; Richardson et al. 2011) is similar to that of Crater II ($M_V = -8.5$ mag), but the spatial extent of And XXIV is smaller ($r_h = 680$ kpc). However, no search for variable stars has been performed in And XXIV, and the data of Martin et al. (2017) cover about 36 per cent of its extent. A deeper analysis of the SFH and the stellar content of this galaxy would be of extreme interest to compare with Crater II.

The HB morphology of Crater II becomes even more peculiar when compared with HB morphologies of Galactic GCs. Indeed, GCs with metal abundances in the range $-1.9 <$ [Fe/H] < -1.5 present a predominantly blue HB (e.g. NGC 6535, NGC 6144, and NGC 6541), or a redder morphology but still with a well-populated blue part (e.g. NGC 7006, NGC 5272). The few clusters with entirely red HBs do not host any RRL (e.g. AM 1, Palomar 14, Pyxis), unlike the case for Crater II. Possibly, the only GC with HB resembling that of Crater II is the peculiar Ruprecht 106 (Kaluzny et al. 1995; Dotter, Sarajedini & Anderson 2011). This is one of the very few GCs that does not display chemical abundance variations typical of multiple populations (Villanova et al. 2013; Bastian & Lardo 2017). Moreover and even more importantly, Ruprecht 106 has also the remarkable feature of not presenting enhancement in the α-elements (Villanova et al. 2013). This means that the empirical scenario becomes even more puzzling, since dwarf galaxies in the metal-poor regime ([Fe/H]≤ -1.5) display a well defined α-enhancement (Cohen & Huang 2009; Hendricks et al. 2014; Fabrizio et al. 2015).

The current empirical evidence indicates that the HB morphology of Crater II is too red for its metallicity. The paucity of blue HB stars, once confirmed, is a real conundrum, since theory and observations are suggesting that the metal content is the main parameter in driving the HB morphology (Salaris & Cassisi 2005). The lack of blue HB stars is an additional indication that the very metal-poor ($Z < 0.0003$) component of Crater II is small, if present. We are therefore presented with a peculiarly very extended, relatively faint and low surface brightness galaxy with, however, not extremely low mean metallicity, but low metallicity dispersion and possibly lacking a tail toward extremely metal-poor stars typical of galaxies of similar brightness.

What mechanisms may have originated a dwarf with a peculiar HB morphology, a low metallicity dispersion and possibly lacking of extremely metal-poor stars?

Caldwell et al. (2017) found a far too low central velocity dispersion ($\sigma_v = 2.7$ Km s^{-1}), difficult to explain within the standard Λ cold dark matter scenario given the galaxy's observed large size and moderate luminosity. To overcome this, it has been suggested that strong mass-loss ($\sim$90 per cent) must have occurred in Crater II (Fattahi et al. 2018; Sanders, Evans & Dehnen 2018). This prediction appears in good agreement with the first orbit determination based on Gaia DR2 (Fritz et al. 2018), which supports that Crater II is on a relatively eccentric orbit with pericentre close to 20 kpc. As a result, Crater II may have already experienced a few passages through denser MW regions. The earliest pericentric passage(s) may have stripped the oldest, most metal-poor component, while the galaxy must have been massive enough to avoid total tidal disruption and keep sufficient mass to undergo further star formation which would have given rise to the moderately metal-rich population currently seen in the center of the galaxy where we have sampled (within half its r_h). This scenario is similar to the one that can be inferred for the dSph galaxy based on the stellar composition and SFHs at different positions along its tidal stream (Martínez-Delgado et al. 2004; de Boer, Belokurov & Koposov 2015).

However, population gradients are commonly observed in LG dwarf galaxies (Harbeck et al. 2001; Tolstoy et al. 2004; Bernard et al. 2008; Martínez-Vázquez et al. 2015, 2016a), in the sense that the younger/more metal-rich components are more centrally concentrated (and this is reflected in the HB getting bluer when moving to the external regions). Additionally, deeper data will allow

Downloaded from https://academic.oup.com/mnras/article/479/4/4279/5046475 by CNRS - ISTO user on 07 June 2022

us to put more stringent limits on the possible duration of the star formation epoch. These new data are thus necessary to put stronger constraints on the properties of the old populations of this galaxy and their possible radial gradients. The existence (or not) of a very metal-poor population at larger galactocentric radius will help constrain its early evolution, the possible effects of early stripping episodes, and therefore even its history of interactions with the MW, and thus possibly its orbit. The stellar distribution in a large area may also reveal the presence of tidal tails, which, however, may be challenging to detect due to the extremely low surface brightness.

ACKNOWLEDGEMENTS

This research has been supported by the Spanish Ministry of Economy and Competitiveness (MINECO) under the grant AYA2014-56795-P. This research has made use of the NASA/IPAC Extragalactic Database (NED) which is operated by the Jet Propulsion Laboratory, California Institute of Technology, under contract with the National Aeronautics and Space Administration. This article is based on observations made in the Observatorios de Canarias del IAC with the INT operated on the island of La Palma by the Isaac Newton Group in the Observatorio del Roque de los Muchachos.

REFERENCES

Alcock C. et al., 2000, AJ, 119, 2194
Arellano Ferro A., Rojas López V., Giridhar S., Bramich D. M., 2008, MNRAS, 384, 1444
Bastian N., Lardo C., 2017, preprint (arXiv:1712.01286)
Bechtol K. et al., 2015, ApJ, 807, 50
Bernard E. J. et al., 2008, ApJ, 678, L21
Bernard E. J. et al., 2009, ApJ, 699, 1742
Bono G., 2003, in Alloin D., Gieren W., eds, Lecture Notes in Physics Vol. 635, Stellar Candles for the Extragalactic Distance Scale. Springer-Verlag, Berlin, p. 85
Bono G., Caputo F., Santolamazza P., Cassisi S., Piersimoni A., 1997, AJ, 113, 2209
Bono G., Caputo F., Castellani V., Marconi M., Storm J., 2001, MNRAS, 326, 1183
Bono G., Caputo F., Castellani V., Marconi M., Storm J., Degl'Innocenti S., 2003, MNRAS, 344, 1097
Braga V. F. et al., 2016, AJ, 152, 170
Cacciari C., Clementini G., 2003, in Alloin D., Gieren W., eds, Lecture Notes in Physics Vol. 635, Stellar Candles for the Extragalactic Distance Scale. Springer-Verlag, Berlin, p. 105
Cacciari C., Corwin T. M., Carney B. W., 2005, AJ, 129, 267
Caldwell N. et al., 2017, ApJ, 839, 20
Carretta E., Gratton R. G., Clementini G., Fusi Pecci F., 2000, ApJ, 533, 215
Cassisi S., Potekhin A. Y., Pietrinferni A., Catelan M., Salaris M., 2007, ApJ, 661, 1094
Chaboyer B., 1999, post-Hipparco Distance Determinations, 237, 111
Clementini G., Gratton R., Bragaglia A., Carretta E., Di Fabrizio L., Maio M., 2003, AJ, 125, 1309
Clementini G., Cignoni M., Contreras Ramos R., Federici L., Ripepi V., Marconi M., Tosi M., Musella I., 2012, ApJ, 756, 108
Cohen J. G., Huang W., 2009, ApJ, 701, 1053
Coppola G. et al., 2015, ApJ, 814, 71
Cusano F. et al., 2013, ApJ, 779, 7
Cusano F. et al., 2016, ApJ, 829, 26
Cusano F. et al., 2017, ApJ, 851, 9
Da Costa G. S., Armandroff T. E., Caldwell N., Seitzer P., 1996, AJ, 112, 2576
Da Costa G. S., Armandroff T. E., Caldwell N., Seitzer P., 2000, AJ, 119, 705
Da Costa G. S., Armandroff T. E., Caldwell N., 2002, AJ, 124, 332
de Boer T. J. L., Belokurov V., Koposov S., 2015, MNRAS, 451, 3489
de Grijs R., Courbin F., Martínez-Vázquez C. E., Monelli M., Oguri M., Suyu S. H., 2017, Space Sci. Rev., 212, 1743
Di Criscienzo M., Caputo F., Marconi M., Cassisi S., 2007, A&A, 471, 893
di Criscienzo M. et al., 2011, MNRAS, 414, 3381
Di Criscienzo M. et al., 2011, AJ, 141, 81
Dotter A., Sarajedini A., Anderson J., 2011, ApJ, 738, 74
Drlica-Wagner A. et al., 2015, ApJ, 813, 109
Drlica-Wagner A. et al., 2016, ApJ, 833, L5
Fabrizio M. et al., 2015, A&A, 580, A18
Fattahi A., Navarro J. F., Frenk C. S., Oman K. A., Sawala T., Schaller M., 2018, MNRAS, 476, 3816
Fiorentino G., Monelli M., 2012, A&A, 540, A102
Fiorentino G. et al., 2015, ApJ, 798, L12
Fiorentino G. et al., 2017, A&A, 599, A125
Fritz T. K., Battaglia G., Pawlowski M. S., Kallivayalil N., van der Marel R., Sohn T. S., Brook C., Besla G., 2018, preprint (arXiv:1805.00908)
Harbeck D. et al., 2001, AJ, 122, 3092
Hendricks B., Koch A., Lanfranchi G. A., Boeche C., Walker M., Johnson C. I., Peñarrubia J., Gilmore G., 2014, ApJ, 785, 102
Horne J. H., Baliunas S. L., 1986, ApJ, 302, 757
Joo S.-J. et al., 2018, ApJ, 861, 23
Kaluzny J., Kubiak M., Szymanski M., Udalski A., Krzeminski W., Mateo M., 1995, A&AS, 112, 407
Kim D., Jerjen H., 2015a, ApJ, 799, 73
Kim D., Jerjen H., 2015b, ApJ, 808, L39
Kim D., Jerjen H., Milone A. P., Mackey D., Da Costa G. S., 2015, ApJ, 803, 63
Kirby E. N., Simon J. D., Geha M., Guhathakurta P., Frebel A., 2008, ApJ, 685, L43
Koposov S. et al., 2008, ApJ, 686, 279
Koposov S. E., Belokurov V., Torrealba G., Evans N. W., 2015, ApJ, 805, 130
Koposov S. E. et al., 2018, MNRAS (arXiv:1804.06430)
Kunder A. et al., 2013, AJ, 146, 119
Laevens B. P. M. et al., 2015a, ApJ, 802, L18
Laevens B. P. M. et al., 2015b, ApJ, 813, 44
Layden A. C., Ritter L. A., Welch D. L., Webb T. M. A., 1999, AJ, 117, 1313
Li T. S. et al., 2017, ApJ, 838, 8
Longmore A. J., Fernley J. A., Jameson R. F., 1986, MNRAS, 220, 279
Madore B. F., 1982, ApJ, 253, 575
Mapelli M., Ripamonti E., Tolstoy E., Sigurdsson S., Irwin M. J., Battaglia G., 2007, MNRAS, 380, 1127
Mapelli M., Ripamonti E., Battaglia G., Tolstoy E., Irwin M. J., Moore B., Sigurdsson S., 2009, MNRAS, 396, 1771
Marconi M. et al., 2015, ApJ, 808, 50
Martin N. F., Ibata R. A., Irwin M., 2007, ApJ, 668, L123
Martin N. F. et al., 2015, ApJ, 804, L5
Martin N. F. et al., 2017, ApJ, 850, 16
Martínez-Delgado D., Gómez-Flechoso M. Á., Aparicio A., Carrera R., 2004, ApJ, 601, 242
Martínez-Vázquez C. E. et al., 2015, MNRAS, 454, 1509
Martínez-Vázquez C. E. et al., 2016a, MNRAS, 461, L41
Martínez-Vázquez C. E. et al., 2016b, MNRAS, 462, 4349
Martínez-Vázquez C. E. et al., 2017, ApJ, 850, 137
Mateo M. L., 1998, ARA&A, 36, 435
Mateo M., Fischer P., Krzeminski W., 1995, AJ, 110, 2166
McConnachie A. W. et al., 2008, ApJ, 688, 1009
McNamara D. H., 2011, AJ, 142, 110
Monelli M. et al., 2003, AJ, 126, 218
Monelli M. et al., 2012a, MNRAS, 422, 89
Monelli M. et al., 2012b, ApJ, 744, 157
Pietrinferni A., Cassisi S., Salaris M., Castelli F., 2004, ApJ, 612, 168
Pietrinferni A., Cassisi S., Salaris M., Castelli F., 2006, ApJ, 642, 797
Richardson J. C. et al., 2011, ApJ, 732, 76

Downloaded from https://academic.oup.com/mnras/article/479/4/4279/5046475 by CNRS - ISTO user on 07 June 2022

Salaris M., Cassisi S., 2005, Evolution of Stars and Stellar Populations, Wiley-VCH, New York, p. 400
Sandage A., Katem B., Sandage M., 1981, ApJS, 46, 41
Sanders J. L., Evans N. W., Dehnen W., 2018, MNRAS, 478, 3879
Santana F. A., Muñoz R. R., Geha M., Côté P., Stetson P., Simon J. D., Djorgovski S. G., 2013, ApJ, 774, 106
Schlafly E. F., Finkbeiner D. P., 2011, ApJ, 737, 103
Sesar B. et al., 2017, AJ, 153, 204
Siegel M. H., 2006, ApJ, 649, L83
Stetson P. B., 1996, PASP, 108, 851
Stetson P. B., 2000, PASP, 112, 925
Stetson P. B., 2005, PASP, 117, 563
Stetson P. B., Fiorentino G., Bono G., Bernard E. J., Monelli M., Iannicola G., Gallart C., Ferraro I., 2014, PASP, 126, 616
Tolstoy E. et al., 2004, ApJ, 617, L119
Tolstoy E., Hill V., Tosi M., 2009, ARA&A, 47, 371
Torrealba G., Koposov S. E., Belokurov V., Irwin M., 2016a, MNRAS, 459, 2370
Torrealba G. et al., 2016b, MNRAS, 463, 712
Torrealba G. et al., 2018, MNRAS, 475, 5085
Villanova S., Geisler D., Carraro G., Moni Bidin C., Muñoz C., 2013, ApJ, 778, 186
Walker A. R., 1989, AJ, 98, 2086
Welch D. L., Stetson P. B., 1993, AJ, 105, 1813
Yang S.-C., Sarajedini A., 2012, MNRAS, 419, 1362
Yang S.-C., Wagner-Kaiser R., Sarajedini A., Kim S. C., Kyeong J., 2014, ApJ, 784, 76

SUPPORTING INFORMATION

Supplementary data are available at *MNRAS* online.

Please note: Oxford University Press is not responsible for the content or functionality of any supporting materials supplied by the authors. Any queries (other than missing material) should be directed to the corresponding author for the article.

APPENDIX: ONLINE MATERIAL

Time series photometry for detected variable stars in the central regions of Crater II is listed in Table A1. The table presents, for each star, the modified Heliocentric Julian Date of mid-exposure (HJD – 2400 000, columns 1, 4, 7), individual *B*, *V*, and *I* measurements (columns 2, 5, 8) and their uncertainties (columns 3, 6, 9). The full version of the table is available on the online version of the paper.

Downloaded from https://academic.oup.com/mnras/article/479/4/4279/5046475 by CNRS - ISTO user on 07 June 2022

Table A1. Photometryof the variable stars in Crater II dSph.

MHJD∗	B	σ_B	MHJD∗	V	σ_V	MHJD∗	I	σ_I
				CraterII-V001				
57538.3730	20.862	0.192	57538.4276	20.737	0.023	57538.4312	20.069	0.039
57538.4249	21.214	0.028	57540.4067	20.227	0.016	57540.4102	19.839	0.028
57539.4280	21.318	0.036	57540.4395	20.306	0.014	57540.4137	19.769	0.030
57540.4039	20.486	0.018	57541.4030	20.631	0.021	57540.4430	19.812	0.024
57540.4368	20.606	0.021	57541.4296	20.647	0.018	57541.4077	19.998	0.024
57541.4002	21.062	0.023	57847.4935	20.620	0.026	57541.4269	20.003	0.027
57541.4324	21.147	0.024	57847.5050	20.650	0.025	57781.6373	19.832	0.026
57781.6234	20.647	0.016	57847.5247	20.675	0.027	57781.6801	19.797	0.016
57781.6678	20.792	0.012	57847.5465	20.688	0.034	57781.6968	19.868	0.014
57781.6848	20.828	0.011	57847.5664	20.738	0.034	57781.7140	19.840	0.015
57781.7017	20.865	0.011	57847.5873	20.712	0.028	57781.7300	19.856	0.013
57781.7190	20.893	0.013	57847.6049	20.804	0.029	57781.7525	19.910	0.019
57781.7395	20.939	0.014	57848.4812	20.864	0.043	57782.6171	19.942	0.032
57781.7570	20.994	0.019	57848.4992	20.761	0.042	57782.6321	19.953	0.024
57782.6106	21.170	0.022	57848.5345	20.730	0.040	57782.6459	20.018	0.023
57782.6235	21.136	0.019	57848.5526	20.878	0.044	57782.6573	20.073	0.021
57782.6381	21.165	0.018	57848.5747	20.867	0.047	57782.6688	20.037	0.018
57782.6502	21.204	0.016	57848.5940	20.954	0.047	57782.6802	20.017	0.021
57782.6616	21.204	0.015	57849.4671	20.083	0.037	57782.6917	20.085	0.027
57782.6731	21.248	0.016	57849.4869	20.101	0.035	57782.7031	20.109	0.024
57782.6845	21.232	0.015	57849.5126	20.162	0.034	57782.7145	20.070	0.023
57782.6959	21.237	0.015	57849.5337	20.218	0.040	57782.7260	20.099	0.020
57782.7073	21.252	0.016	57849.5537	20.201	0.042	57782.7374	20.134	0.028
57782.7188	21.286	0.016	57849.5724	20.355	0.051	57782.7488	20.075	0.022
57782.7303	21.280	0.015	57849.5910	20.286	0.050	57782.7605	20.104	0.023
57782.7417	21.305	0.017	–	–	9.999	57782.7719	20.093	0.033
57782.7533	21.300	0.018	–	–	9.999	57800.5651	19.951	0.041
57782.7648	21.286	0.021	–	–	9.999	57800.5723	19.844	0.035
57847.4876	21.053	0.046	–	–	9.999	57800.5763	19.874	0.028
57847.4975	21.110	0.048	–	–	9.999	57800.5803	19.823	0.030
57847.5013	21.094	0.046	–	–	9.999	57800.5843	19.825	0.029
57847.5208	21.178	0.043	–	–	9.999	57800.5884	19.729	0.026
57847.5425	21.196	0.050	–	–	9.999	57800.5924	19.723	0.022
57847.5625	21.142	0.046	–	–	9.999	57800.5964	19.656	0.028
57847.5833	21.249	0.049	–	–	9.999	57800.6004	19.701	0.029
57847.6010	21.248	0.033	–	–	9.999	57800.6044	19.671	0.028
57848.4773	21.211	0.059	–	–	9.999	57800.6085	19.647	0.029
57848.4952	21.181	0.072	–	–	9.999	57800.6141	19.635	0.025
57848.5130	21.173	0.071	–	–	9.999	57800.6182	19.645	0.028
57848.5305	21.084	0.060	–	–	9.999	57800.6222	19.666	0.028
57848.5487	21.262	0.064	–	–	9.999	57800.6262	19.715	0.031
57848.5707	21.373	0.072	–	–	9.999	57800.6302	19.693	0.029
57848.5900	21.339	0.069	–	–	9.999	57800.6342	19.693	0.031
57849.4631	20.306	0.048	–	–	9.999	57800.6382	19.666	0.029
57849.4830	20.259	0.041	–	–	9.999	57800.6422	19.685	0.031
57849.5086	20.284	0.051	–	–	9.999	57800.6462	19.689	0.029
57849.5298	20.473	0.057	–	–	9.999	57800.6503	19.692	0.031
57849.5497	20.509	0.063	–	–	9.999	57800.6543	19.712	0.030
57849.5685	20.507	0.060	–	–	9.999	57800.6583	19.717	0.029
57849.5870	20.657	0.073	–	–	9.999	57800.6623	19.727	0.032
–	–	9.999	–	–	9.999	57800.6663	19.752	0.032
–	–	9.999	–	–	9.999	57800.6703	19.700	0.032
–	–	9.999	–	–	9.999	57800.6744	19.653	0.031
–	–	9.999	–	–	9.999	57800.6784	19.804	0.032
–	–	9.999	–	–	9.999	57800.6824	19.782	0.027
–	–	9.999	–	–	9.999	57800.6864	19.715	0.033
–	–	9.999	–	–	9.999	57800.6904	19.755	0.036
–	–	9.999	–	–	9.999	57800.6945	19.759	0.034
–	–	9.999	–	–	9.999	57800.6985	19.744	0.030
–	–	9.999	–	–	9.999	57800.7026	19.819	0.040
–	–	9.999	–	–	9.999	57800.7066	19.760	0.034
–	–	9.999	–	–	9.999	57800.7106	19.756	0.036
–	–	9.999	–	–	9.999	57800.7146	19.714	0.035
–	–	9.999	–	–	9.999	57800.7186	19.758	0.035

This paper has been typeset from a TEX/LATEX file prepared by the author.

Downloaded from https://academic.oup.com/mnras/article/479/4/4279/5046475 by CNRS - ISTO user on 07 June 2022